Electromagnetic Wave Propagation in Salt—Probing into Salt with Radar[1]

R. R. Unterberger
Department of Geophysics
Texas A&M University
College Station, Texas 77843

ABSTRACT

From electromagnetic wave theory it is clear that the attenuation of a wave through any material will depend on two factors μ^* and ϵ^*, the complex magnetic permeability and the complex permittivity, respectively. Both of these parameters (of any material or rock) have a real and an imaginary part e.g. $\epsilon^* = \epsilon' - j\epsilon''$. The imaginary part determines the attenuation, the real part determines the wave velocity. Salt, in either piercement salt domes or bedded deposits, is nonmagnetic and so $\mu^* = \mu_0$, the magnetic permeability of free space, and $\mu'' = 0$, i.e. salt is magnetically lossless. The question is, is salt lossless in the electrical sense?

To determine theoretically if electromagnetic waves will propagate through salt we have measured the tan δ (defined as ϵ''/ϵ') of various rock salt samples and found that dry salt, such as that found in Gulf Coast piercement salt domes, has a low loss tangent. Tan δ's measured on some rock salt have been equal to that of teflon and polyethylene, materials used in coaxial cables to transmit electromagnetic waves. One rock salt sample, measured by the National Bureau of Standards, yielded a tan $\delta = 2 \times 10^{-5}$ which is a factor of 5 lower than teflon.

Pulsed and CW-FM radars of various frequencies have been used to probe into salt in salt mines to "see ahead" of mining to determine whether hazards to mining exist. Such hazards may be an abandoned, unplugged well that connects with an aquifer at some level above the mine. Any discontinuities in rock material contacts, such as salt to water, salt to sand, salt to anhydrite, cause a reflection of the radar waves. The return energy is measured in time and a knowledge of the wave velocity determines the range in salt to this discontinuity. In general, salt miners are interested in anything that is not salt as it represents a problem to them: a minor problem if a small impurity, a major problem if a source of high pressure water.

The ability to penetrate salt with radar in a number of salt mines has been demonstrated. Locations of the flanks of salt domes have been accomplished using radar techniques from within the salt mine.

Data are shown indicating the high-resolution, short-range detection capability of a CW-FM microwave radar. Radar has been used to probe through salt and from the data the top of a tunnel in salt has been plotted by "looking through" the floor of the salt from above.

INTRODUCTION

This paper is divided into two parts. The first part contains the theory of electromagnetic wave propagation in salt showing why the complex electric permittivity of salt is important and how it controls our ability to detect discontinuities in salt. The second part discusses results accomplished in the various salt mines visited for research tests. For those not interested in the theoretical part it is suggested that part I be bypassed.

PART I. THEORY

All electromagnetic wave propagation is based on Maxwell's equations. This paper uses the rationalized MKS system of units. Thus, we have Maxwell's equations in vector form. With an underline the terms indicate a vector; other parameters not underlined are scalars,

$$\nabla \cdot \underline{D} = \rho \tag{1}$$

$$\nabla \cdot \underline{B} = 0 \tag{2}$$

1. This research is sponsored through the Solution Mining Research Institute by the following salt companies listed in alphabetical order: Canadian Salt Company, Cargill, Inc., Diamond Crystal Salt Company, International Salt Company, Morton Salt Division of Morton International, Sifto Salt Division of Domtar Chemicals, Ltd, and the United Salt Corporation. Solvay et Cie of Brunels recently joined.

$$\nabla \times \underline{E} = -\frac{\partial \underline{B}}{\partial t} \tag{3}$$

$$\nabla \times \underline{H} = \underline{J} + \frac{\partial \underline{D}}{\partial t} \tag{4}$$

Equation (1) is a statement of Gauss's law, whereas (2) expresses the continuity of $\underline{B}$, the magnetic flux density. Equation (3) is Faraday's law in vector form and forms the basis for the majority of the power generating capacity of the world. Equation (4) is Ampere's law as modified by Maxwell who introduced the concept of displacement current, which is the last term on the right side of (4). Without this term he would not have shown the regenerative nature of the electromagnetic waves: a changing $\underline{D}$ generates an $\underline{H}$, and a changing $\underline{H}$ (or $\underline{B}$) generates an $\underline{E}$ (or $\underline{D}$).

For completeness, the symbols in the above equations are defined with their units:

$\underline{D}$ = electric displacement vector in coulomb per meter squared, C/m^2

ρ = electric charge density in coulomb per meter cubed, C/m^3

$\underline{B}$ = magnetic flux density in tesla, T*

$\underline{E}$ = electric field intensity in volt per meter, V/m

$\underline{H}$ = magnetic field intensity in ampere per meter, A/m

$\underline{J}$ = current density in ampere per meter squared, A/m^2

Other equations necessary to development of the theory are:

$$\underline{B} = \mu \underline{H} \tag{5}$$

$$\underline{D} = \epsilon \underline{E} \tag{6}$$

$$\underline{J} = \sigma \underline{E} \tag{7}$$

$$\underline{F} = q\underline{E} + q(\underline{v} \times \underline{B}) \tag{8}$$

$$\mu_0 = 4\pi \times 10^{-7}\ \text{H/m} \tag{9}$$

$$\epsilon_0 = 8.85 \times 10^{-12}\ \text{F/m} \tag{10}$$

Equations (5) and (6) are called the constitutive equations. (5) relates the two magnetic vectors through the magnetic permeability μ of material or μ_0 for free space. (6) does the same for the two electric vectors. Equation (7) is a vector statement of Ohm's law where σ is the conductivity of the material in siemens (S), the U.S. National Bureau of Standard's approved term for mho. Equation (8) is the Lorentz equation with the force $\underline{F}$ in newtons, the charge q in coulombs, and the vector velocity $\underline{v}$ in meter per second. Note in equations (9) and (10) the magnetic permeability, μ_0, and the electric permittivity, ϵ_0, of free space have values as well as units. This is in contrast with the CGS or Gaussian system of units.

Interest shall be focused on the relative value of conduction current $\underline{J}$ and displacement current $\partial \underline{D}/\partial t$ because it is this that determines whether a material (salt in this case) is a conductor or a dielectric. Substituting (7) into (4) and (6) into (4) one obtains

$$\nabla \times \underline{H} = \sigma \underline{E} + j\omega\epsilon\, \underline{E} \tag{11}$$

and the ratio $\sigma/\omega\epsilon$ becomes important. If

$$\frac{\sigma}{\omega\epsilon} > 100 \tag{12}$$

the material is a conductor. If

$$\frac{\sigma}{\omega\epsilon} < \frac{1}{100} \tag{13}$$

the material is a dielectric. Intermediate values are semiconductors.

Next consider deriving the wave equation and how the μ and the ϵ of materials fit into the picture of velocity of the electromagnetic wave through salt. Using equations (3) and (5) one obtains

$$\nabla \times \underline{E} = -\mu \frac{\partial \underline{H}}{\partial t} \tag{14}$$

and substituting into (14) equation (4) with no conduction current, i.e. $J = 0$, one obtains, after taking the curl of both sides,

$$\nabla \times \nabla \times \underline{E} = -\mu \frac{\partial}{\partial t}(\nabla \times \underline{H}) \tag{15}$$

$$= -\mu\epsilon \frac{\partial^2 \underline{E}}{\partial t^2} \tag{16}$$

By use of vector identity

$$\times \nabla \times \underline{E} = \nabla(\nabla \cdot \underline{E}) - \nabla \cdot \nabla \underline{E} \tag{17}$$

and knowing that there is no free charge density ρ, so $\nabla \cdot \underline{E} = 0$, one gets the wave equation

$$\nabla^2 \underline{E} = \mu\epsilon \frac{\partial^2 \underline{E}}{\partial t^2} \tag{18}$$

in $\underline{E}$ with a similar one for $\underline{H}$ being easily obtained.

Next consider a complex electric permittivity defined as

$$\boxed{\epsilon^* \equiv \epsilon' - j\epsilon''} \tag{19}$$

Using equation (4) plus equation (7), Ohm's law, and constitutive equation (6) one gets

$$\nabla \times \underline{H} = \sigma \underline{E} + \epsilon \frac{\partial \underline{E}}{\partial t} \tag{20}$$

*One tesla = one weber per meter squared.

which now *includes* the conductivity of the medium. Assuming a sinusoidal driving function

$$\underline{E} = \underline{E}_0 e^{j\omega t} \tag{21}$$

(20) becomes

$$\nabla \times \underline{H} = \sigma \underline{E} + \epsilon j\omega \underline{E} \tag{22}$$

$$= j\omega\epsilon \left(1 + \frac{\sigma}{j\omega\epsilon}\right)\underline{E} \tag{23}$$

or

$$\nabla \times \underline{H} = j\omega\epsilon^* \underline{E} \tag{24}$$

where

$$\epsilon = \epsilon' \tag{25}$$

$$\frac{\sigma}{\omega} = \epsilon'' \tag{26}$$

Thus the relation between the conductivity σ and the imaginary part of the complex electric permittivity is given by

$$\boxed{\sigma = \omega\epsilon''} \tag{27}$$

The real part of the electric permittivity will determine the velocity of the electromagnetic wave through salt. Salt in salt mines is about 99% pure with anhydrite being the usual impurity—thus $\mu = \mu_0$ or the relative magnetic permeability = 1. On the other hand the complex part of the electric permittivity will determine the attenuation of the wave as it progresses through salt. Analytically, this shall be shown below.

Another parameter of interest for salt is its loss tangent, or tan δ.

Consider the simple circuit shown at the right. A sinusoidal generator of voltage $V = V_0 e^{j\omega t}$ feeds a capacitance load C. Now

$$Q \equiv CV \tag{28}$$

is the definition of capacitance. The current I flowing in the circuit is

$$\frac{dQ}{dt} = I_C = C\frac{dV}{dt} = Cj\omega V \tag{29}$$

Note that the charging current, I_C, is 90° out of phase with the driving voltage V as signified by the j multiplied on the right side of (29).

An imperfect capacitance has a resistance R_C, and hence an in-phase current considered as a loss current

$$I_L = \frac{V}{R_C} = GV \tag{30}$$

where G is the conductance. The two currents comprise the total current and the angle δ shown at the right is the loss angle or tan δ of the capacitance. From the two current values it is easily seen that

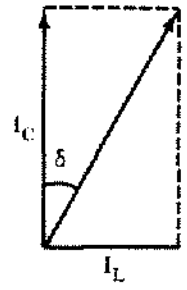

$$\tan\delta = \frac{1}{\omega C R_C} \tag{31}$$

Note that if $R_C \longrightarrow \infty$ then tan $\delta \longrightarrow 0$, i.e., there is a perfect dielectric (no loss) because there is a tan δ of zero. It can also be shown that

$$\boxed{\tan\delta = \frac{\epsilon''}{\epsilon'}} \tag{32}$$

Next consider the wave equation taking into account the conductivity σ. Previously it was considered that $\underline{J} = 0$ which is another way of saying $\sigma = 0$. Here it is not required that it to be equal to zero. The wave equation is then

$$\nabla^2 \underline{E} - \mu\sigma \frac{\partial \underline{E}}{\partial t} - \mu\epsilon \frac{\partial^2 \underline{E}}{\partial t^2} = 0 \tag{33}$$

whose solution is

$$\underline{E} = \underline{E}_0 e^{j\omega t - \gamma z} \tag{34}$$

where

$$\gamma^2 = j\omega\sigma\mu + j^2\omega^2\mu\epsilon \tag{35}$$

or

$$\gamma = j\omega\sqrt{\mu\left(\epsilon - \frac{j\sigma}{\omega}\right)} \tag{36}$$

or

$$\gamma = j\omega\sqrt{\mu^*\epsilon^*} \tag{37}$$

The propagation constant γ is defined as

$$\gamma \equiv \alpha + j\beta \tag{38}$$

where α is the attenuation factor in neper per meter and β is the phase factor in radian per meter.

Putting eq. (38) into (37) and equating imaginary parts and real parts, one obtains, assuming $\mu'' = 0$ (a good assumption for salt because there are no magnetic dipoles in salt nor in its basic impurity anhydrite),

$$\alpha = \omega\sqrt{\frac{\mu'\epsilon'}{2}\left([1 + \tan^2\delta]^{1/2} - 1\right)} \tag{39}$$

$$\beta = \omega\sqrt{\frac{\mu'\epsilon'}{2}\left([1 + \tan^2\delta]^{1/2} + 1\right)} \tag{0}$$

One sees from equation (39) that if one had a perfectly lossless dielectric i.e. tan $\delta = 0$, that the bracket inside the square root sign would be equal to unity and that α would thus reduce to zero. This is the case for a vacuum and thus light can travel without attenuation (except for geometrical spreading).

Radar equation in air

Interest here is focused on the propagation of electromagnetic waves through salt. To do this, electromagnetic waves are launched into salt using a radar system. The situation is much like ordinary radar in air with the exception that one now has to consider attenuation in the transmission medium—salt. (The attenuation of air at radar frequencies is negligible and does not appear in the usual radar equation). The normal radar equation for the received power signal S is

$$S = \left[\frac{P_T G}{4\pi R^2}\right]\left[\frac{\sigma}{4\pi R^2}\right]\left[\frac{G\lambda^2}{4\pi}\right] \tag{41}$$

where

P_T = Peak pulse power transmitted, watt
G = Antenna gain, dimensionless
R = Range to the radar target, meter
σ = Radar back-scattering cross-section, meter squared
λ = Wavelength, meter

Equation (41) can be understood by considering each set of parentheses. The first parenthesis has to do with radar transmitter. The $4\pi R^2$ is simply geometrical spreading. The peak power transmitted is spread over a surface of $4\pi R^2$ except that the antenna gain increases the energy density by a factor G., i.e., the energy spread is *not* isotropic.

The second parenthesis has to do with the radar target. The target (salt discontinuity) has a back-scattering cross-section of σ meters, i.e., an area, that returns energy in the direction to the radar transmitter. A radar target thus has a σ that is very directionally dependent and this σ characterizes this particular target. Although the σ is called back-scattering cross-section it is measured in such a way that it is assumed that the energy is uniformly distributed in all directions. Hence the $4\pi R^2$ geometric spreading factor.

The third parenthesis of equation (41) has to do with the receiving antenna. The energy has been transmitted, it has been back scattered and now must be picked up by the receiving antenna and converted into electrical signal. The capture cross-sectional area A of an antenna is related to its gain G by

$$G = \frac{KA}{\lambda^2}$$

where $K = 4\pi$ usually. The first two parentheses of equation (41) yield units of watts per square meter at the radar system after being reflected from a target at range R and of cross section σ. Multiply this by the capture cross-sectional area A of the antenna and we convert this energy density to received power (watts) resulting in the received power signal S.

Equation (41) can be written more compactly as

$$\boxed{S = \frac{P_T G^2 \lambda^2 \sigma}{(4\pi)^3 R^4}} \tag{42}$$

It is important to note the signal received power S decreases as the *fourth* power of range whereas it increases only linearly with transmitted power P_T. Thus to *double* the radar range one needs to increase the transmitted power by *sixteen* or 2^4. In equation (42) all parameters can be measured easily except σ. This parameter is usually determined for a particular target, a particular aspect angle (direction of viewing), and a particular electromagnetic wave polarization by actual field measurement, either full-scale or modeled.

Radar equation with attenuation

Now one is not so much interested in the radar received signal power S, but how this signal power S compares with the noise power P_N of the radar system. In addition the signal to noise ratio of the received signal, usually expressed in decibels (dB) is important. If now one includes the attenuation of the wave through salt, remembering that the signal has to travel a total length of 2R, and that the attenuation factor α relates to the E vector attenuation (not power), one must square E to get power. Hence

$$S = \frac{P_T G^2 \lambda^2 \sigma}{(4\pi)^3 R^4} e^{-4\alpha R} \tag{43}$$

By virtue of the definition of a decibel as

$$dB = 10 \log \frac{P_1}{P_2} \tag{44}$$

where P_1 and P_2 are two powers, one has

$$\boxed{\frac{S}{N} = 10 \log \frac{P_T G^2 \lambda^2 \sigma}{(4\pi)^3 P_N R^4} e^{\frac{-4\pi R \tan \delta}{\lambda} \sqrt{\frac{\epsilon' \mu'}{\epsilon_0 \mu_0}}}} \tag{45}$$

where the value of α from equation (39) is inserted using the simplifying assumption that tan $\delta < .01$. Is this assumption justified for salt?

Electrical properties of salt samples

In the laboratory, salt samples have been cut to fit a coaxial dielectrometer and measurements of the complex electric permittivity ϵ^* as a function of frequency have been made. Salt samples from various salt mines have different loss tangents or tan δ's, but quite readily fulfill the simplifying assumption made for α in equation (45). To illustrate what an excellent transmitter of VHF electromagnetic wave salt can be, consider one sample from the Grand Saline salt mine in Texas. This sample was taken to the U.S. National Bureau of Standards laboratory in Boulder, Colorado and a tan $\delta = 2 \times 10^{-5}$ was measured. This is a factor of 5 better (lower) than teflon and a factor of 10 better than polyethylene, both of which are common coaxial cable dielectrics chosen particularly for their ability to transmit electromagnetic waves with low attenuation. Other actual salt samples measured had tan δ's between 10^{-4} and 10^{-3} although at lower frequencies the tan δ tended to increase. Care must be taken not to permit water from the air to be absorbed onto the salt sample surface as the dipole moment of water increases the tan δ measured. It is for this reason that in the laboratory all tan δ measurements are made in a dry box.

Figure 1 shows the low-loss frequency region for salt. This is taken from Breckenridge (1947). Figure 2 gives a pictoral representation of an electromagnetic wave traveling from left to right and being attenuated by an imperfect dielectric such as salt. Note that the amplitude of the $\underline{E}$ vector is decreasing to the right as well as oscillating in time. The accompanying $\underline{H}$ vector is at right angles to the $\underline{E}$ vector and in such a direction that $\underline{E} \times \underline{H} = \underline{P}$, where $\underline{P}$ is the transmitted Poynting vector which gives the direction of power flow. The phase angle shown is caused by the finite imaginary parts of ϵ^* or μ^* of the material. This causes the attenuation of the wave. If $\mu'' = \epsilon'' = 0$ there would be no attenuation and the peak amplitude of the plane wave would remain constant.

PART II. RADAR PROBING IN SALT MINES

It has been shown theoretically that if the tan δ of salt is sufficiently low, one can expect to transmit radar through hundreds of feet of salt (we have transmitted through thousands). Let us see what has been accomplished by the putting into practice this theoretical possi-

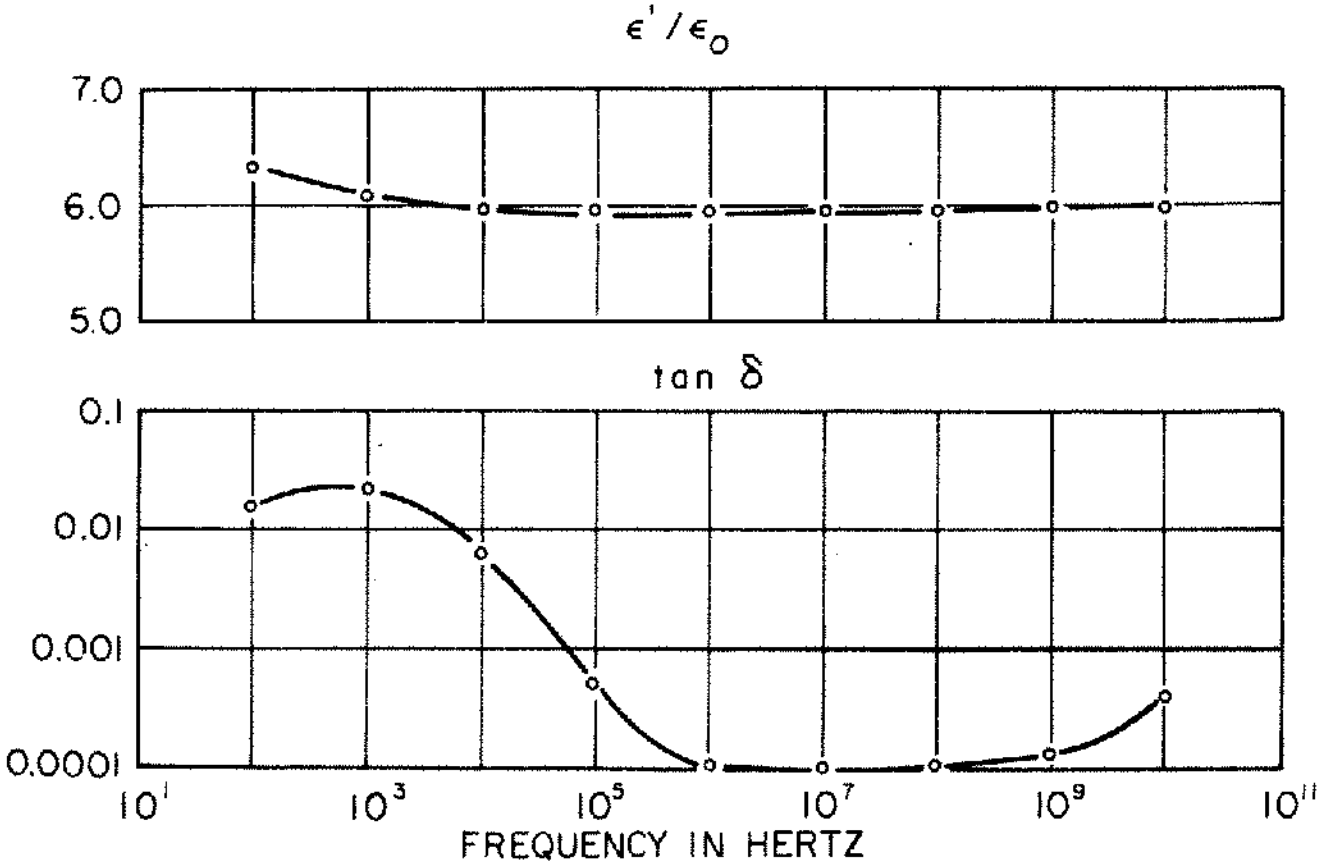

Figure 1. Dielectric Properties of NaCl crystal.

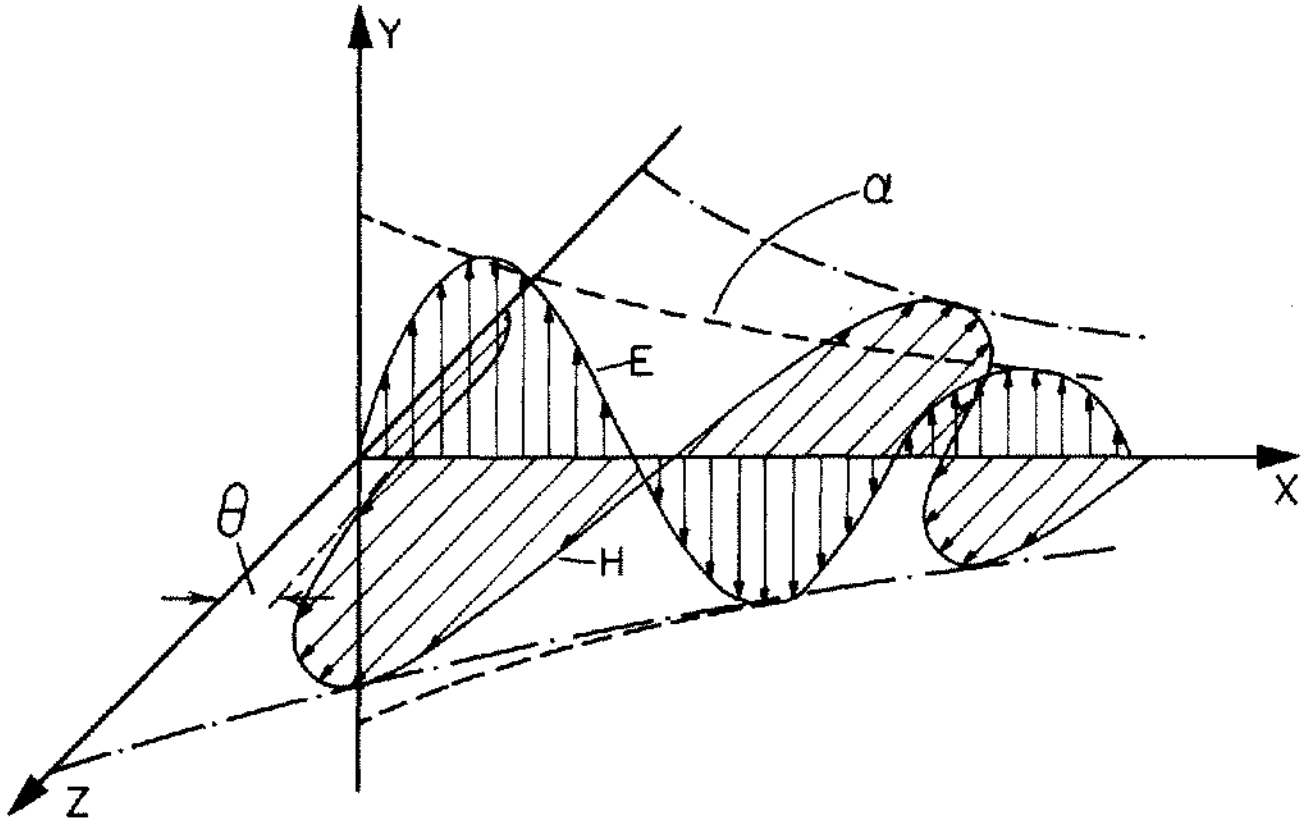

Figure 2. Attenuation of a plane electromagnetic wave in an imperfect dielectric.

bility. There are two "windows" in salt, i.e., low spots in the parameters causing attenuation as a function of frequency (one in the VHF region as shown in Fig. 1) and another in the near infrared as discussed in another paper (Unterberger, in this publication). Here only VHF and microwave radar results obtained by probing into salt are discussed.

Radar systems

Three radar systems are used. One is high power (20kW) and low frequency (230 MHz) which is used for long range targets such as detecting dome flanks or for probing through highly attenuative media such as *wet* salt. A second radar, (Figure 3) is a low power medium frequency (440 MHz) system for general radar probing of salt. The third system utilizes microwaves and is a CW-FM radar system capable of high resolution and ranges down to a few feet. It accomplishes this short range capability at the expense of long range. Radar in salt is analogous to radar in air. One radar cannot do everything. The military radar that looks for missiles taking off from the Soviet Union is a high-power low-frequency radar. The military radar that tracks airplanes or guided missiles for defense is a medium power and high frequency (short wavelength) system to provide good target resolution. The situation in salt is analogous.

A block diagram of one of the radar systems is shown in Figure 3. Advanced instruments using the boxcar integrator and recorder help to dig weak radar signals out of the noise (20 dB).

Grand Saline salt mine radar probe

The Charlie 1 system was used in the Grand Saline, Texas mine of the Morton Salt Co. The mine is at the 700 foot level with the top of the salt 400 feet overhead. Figure 4 shows the radar return signal after traversing 800 feet of salt, 400 feet to the roof and 400 back. This photograph of the oscilloscope screen was taken with the radar receiver gain turned down considerably. When the gain is turned up and thereby increases the reflected signal (Figure 5) one sees that the second reflection from the roof comes in (far right, 4 μs after the initiation of the radar transmitter). The small radar signal seen at the far right has traveled to the roof, back to the salt mine, back to the roof, and back again to the salt mine where it is received by the radar antenna. Thus this signal has traveled a total of 4 X 400 = 1600 feet in salt.

Using the high power radar (the antennas are shown in

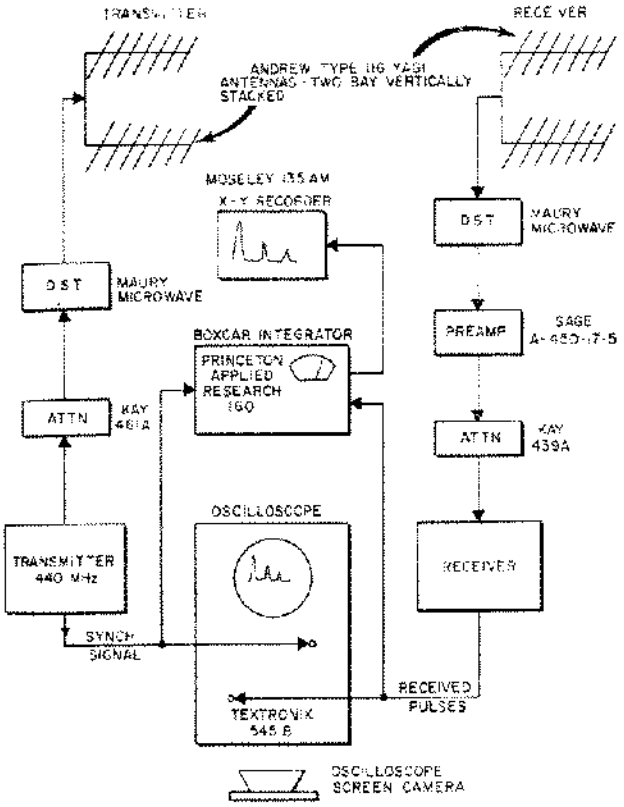

Figure 3. Block Diagram of the Charlie I Radar System.

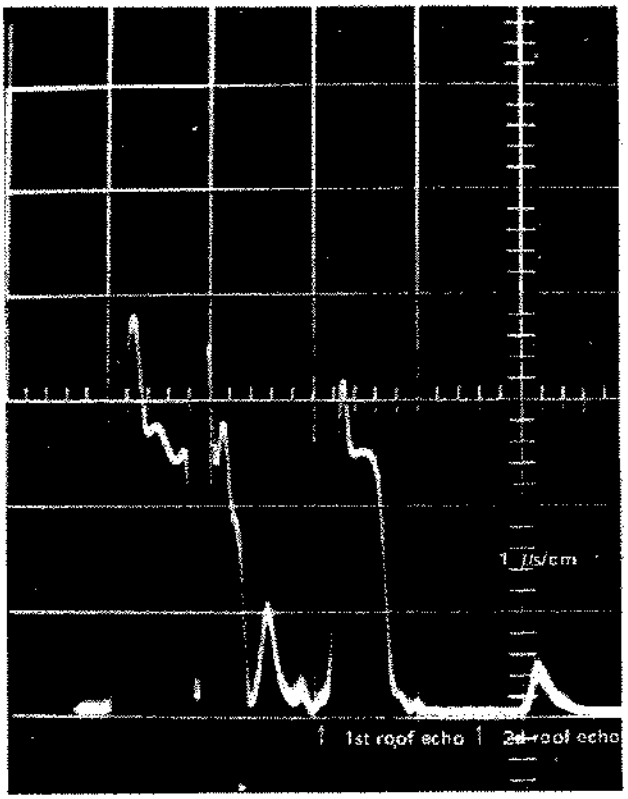

Figure 5. Same as Figure 4 but increased receiver gain.

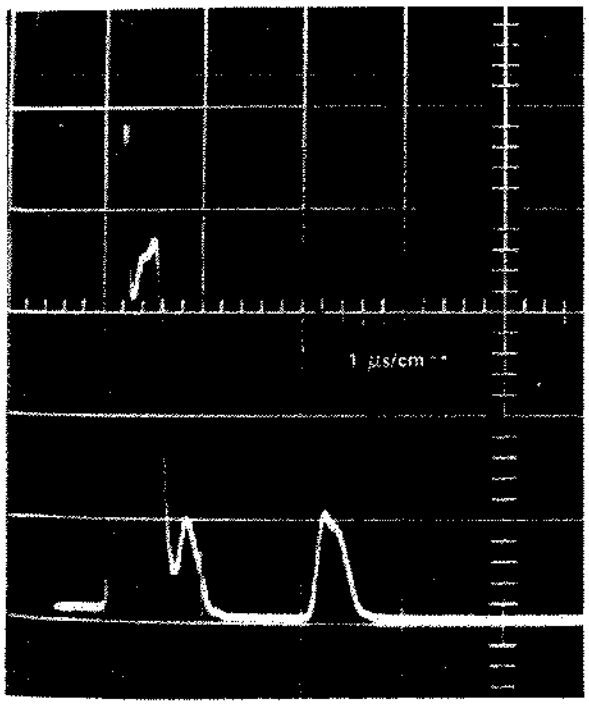

Figure 4. Radar Return from the top of the salt 400 feet above.

Figure 13) one observes a third and fourth echo—the last echo having traversed 3200 feet of salt. Even after 3200 feet of travel through salt, the signal was of sufficient power to be above the noise level of the receiver with no complex signal recovery system (boxcar integrator) needed.

In the same mine it was possible to "look through" a 450 foot pillar of salt and observe the signal received from the salt-air interface of the far wall, (Figure 6). The radar was set up at Station 35 and the antennas were beamed into the salt. Figure 6 shows the radar beam limits. This is slightly misleading because it is at these limits that the beam energy is 3 dB down from the maximum at the beam center. There actually is energy traveling through the salt *outside* the angle indicated by the dotted lines in Figure 6. The purpose of this radar test was *not* to see the other wall of this salt pillar (although it *is* by this type of measurement that one commonly obtains a velocity function which is used to translate radar signals measured in time to distance in salt) but to see a *moving* target on the oscilloscope screen. The moving target was a jeep that was driven by the mine foreman, Mr. Ray Rucker, along the path indicated. A motion picture was taken of the oscilloscope screen. Essentially the screen looked like the photo-

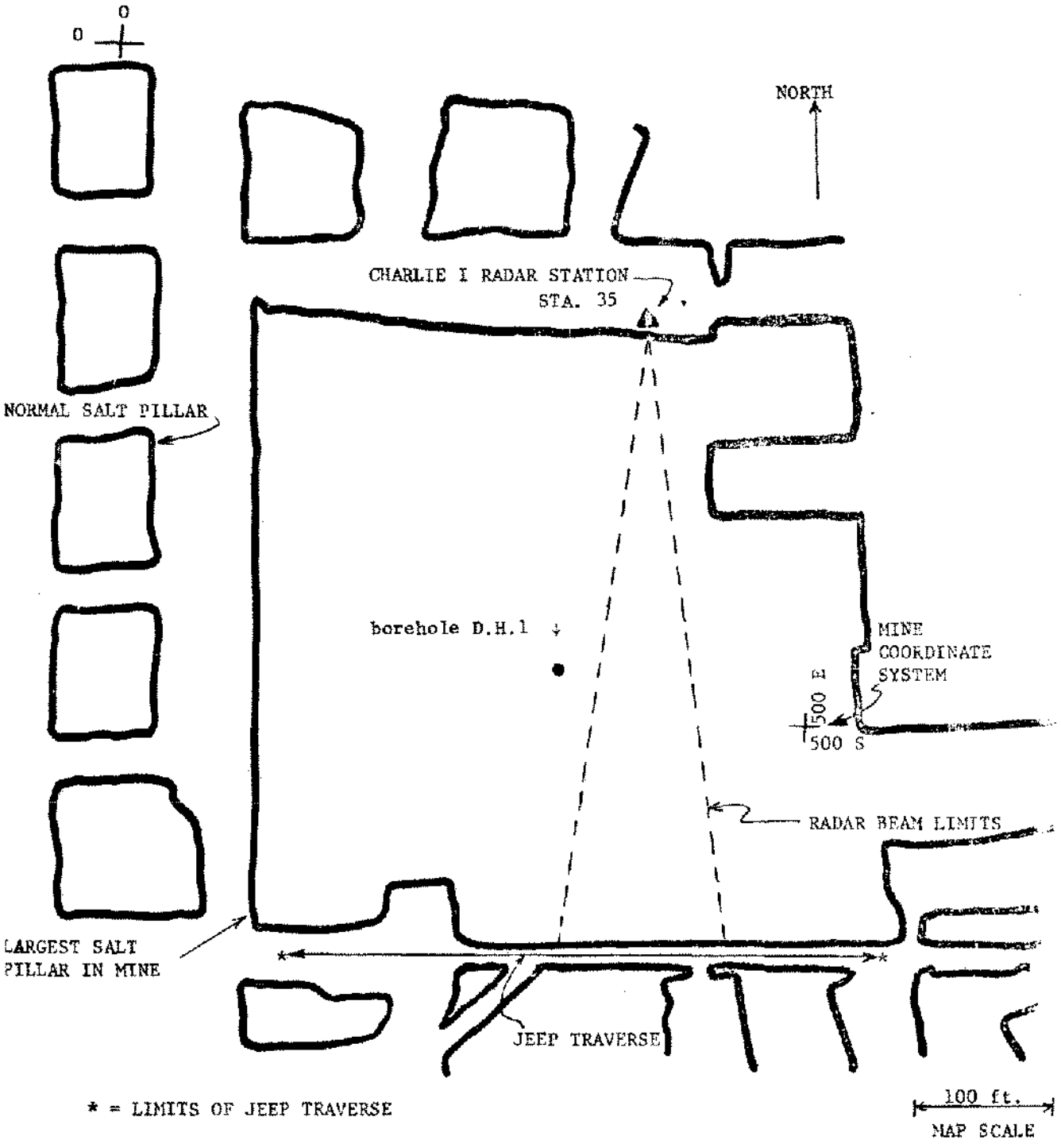

Figure 6. Plan View of Section of Grand Saline Mine.

graph of Figure 7. At the far left is the transmitted (outgoing) pulse. The peak at the right is the radar signal reflected from the salt-air interface forming the south edge of the salt pillar. However the motion picture showed a variation in the height of this peak as a function of time. This was caused by additional radar energy being reflected from the metal side of the jeep as it drove through the radar beam being transmitted *through* this far salt-air interface. The amplitude of the signal received at the radar varied because of the interference pattern derived from a mixture of the two signals—one reflected from the salt-air interface, the other reflected from the air-jeep interface. Both were transmitted back through the salt. A motion picture of the time-varying signal as seen on the oscillo-

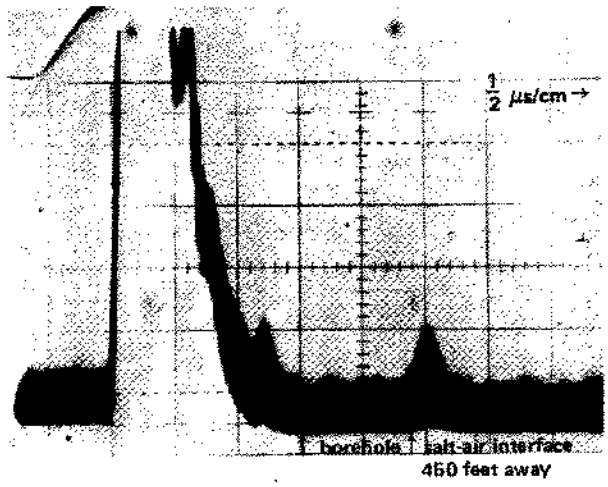

Figure 7. Radar Probing of Salt Pillar.

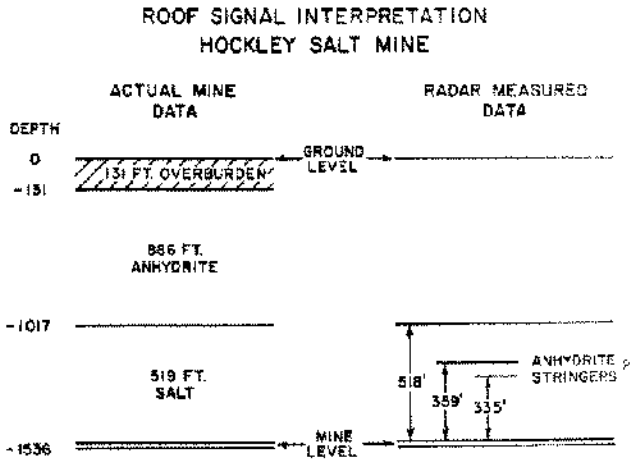

Figure 9. Roof Signal Interpretation, Hockley Salt Mine.

scope screen was shown to those attending the Solution Mining Research Institute meeting in Montreal Canada in May 1970.

Station 35 location was chosen so as to avoid the borehole D.H.1 in the middle of the pillar insofar as possible. It was thought that any water associated with wet salt near the borehole would attenuate the beam and make the objective of seeing through 450 feet of salt more difficult to accomplish. So the Station 35 was chosen as far east as practicable. Although the mission of "seeing" the jeep on the oscilloscope screen was accomplished one also sees the reflected signal from the borehole without trying. That signal is also shown in Figure 7 at 1.3 μs, just after the transmitter pulse. This puts the borehole location 200 feet from radar station 35 which is slightly further north than its location on the salt mine map.

Hockley salt mine radar probe

Recently a survey was made of the three dimensional configuration of the salt-anhydrite interface (top of the salt) from within the Hockley mine. Mr. James A. Hluchanek wrote an M.S. thesis on this research. A paper on this was presented at the International meeting of the Society of Exploration Geophysicists in Mexico City in October 1973. Figure 8 shows a radar signal return oscilloscope presentation. After some reverberation, three radar signals are visible. The interpretation of these signals is as shown in Figure 9. Radar signal A is within one foot of the actual measurement made to this contact in the mine shaft. Radar measured 518 feet; the miners measured 519 feet. This is much closer than can generally be expected. A ten foot error is more probable. Signals B and C are interpreted as reflections from anyhdrite stringers. The actual cause is unknown.

Jefferson Island salt mine radar probe

In this salt mine signals also were observed from the top of the salt (called a roof echo). In certain areas of the mine the reflection from the roof was very large. Figure 10

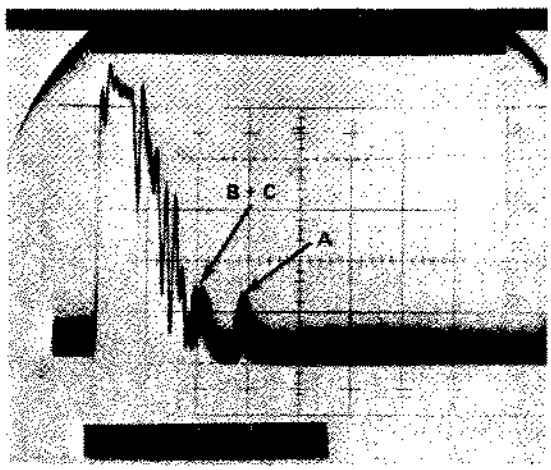

Figure 8. Hockley Salt Mine Radar Data.

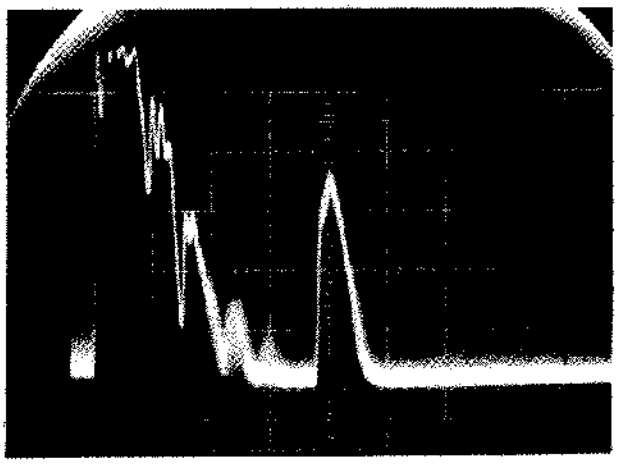

Figure 10. Radar Reflection from Top of Salt from Inside Jefferson Island Mine.

shows a large return signal that is 41 dB above the noise level.

In another area of this salt mine at its lowest level, the radar probing system was moved to a location where it could probe straight up and where there were two pillars directly above us in the upper two mine levels. The test was to see the top of the salt dome by sending radar pulses through the two pillars directly above the location. While the test was unsuccessful in reaching the *top* of the salt with the radar probe, four signals were obtained; one from the 1000 ft mining level, one from the 800 ft mining level and two from other discontinuities in the salt above the top mining level. These signals can be seen in Figure 11. The interpretation of these signals are shown in Figure 12 where the paths of the radar waves should all be superimposed but are *not* for clarity of explanation.

In certain areas where the salt was more lossy, the high powered 230 MHz radar was used. Figure 13 shows the antenna array used with this radar. The antennas are pointing upward to locate the top of the salt. Figure 16 shows the rest of this radar system with Figure 17 showing the oscilloscope and the camera that records the data display.

Salt dome flank locations were also obtained in this salt mine. Radar probing horizontally was done from a number of locations in the mine. Results of this work from four radar stations are shown in Figure 14 where the dome contours obtained from seismic data are compared with the radar data points.

High-resolution, short-range radar probing into salt

All pulse radars suffer from a minimum range problem. That is, one cannot recieve a reflected pulse from a close-in discontinuity and see it on the oscilloscope screen because the transmitted pulse is still on and the energy fed through to the receiver blocks the receiver. To avoid this situation, a CW-FM radar is used. CW means continuous wave. Thus, the transmitter is not pulsed but is on continuously. It is frequency modulated (FM) however. The range to a target is determined by the *difference* in frequency between the signal being received and the instantaneous frequency being transmitted. This is shown in Figure 15 (Luck, 1949; Skolnick, 1962). Such a radar operates at microwave frequencies (4300 MHz) and usually is low power (a few watts). This low power plus the high frequency gives rise to short ranges because the attenuation

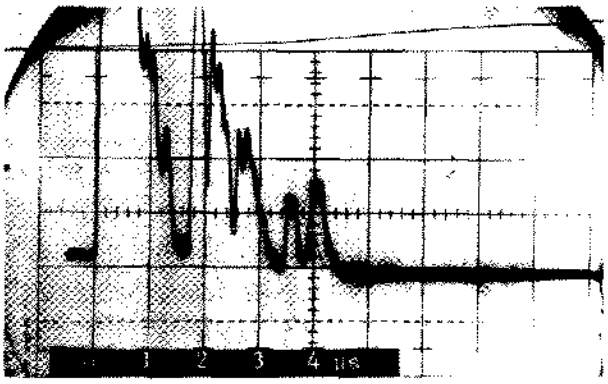

Figure 11. Radar Return, Probing Upward, Jefferson Island Salt Dome.

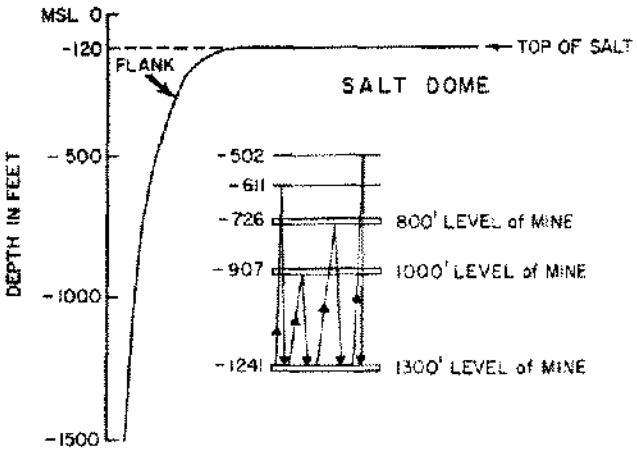

Figure 12. Interpreted Radar Paths, Station G" data.

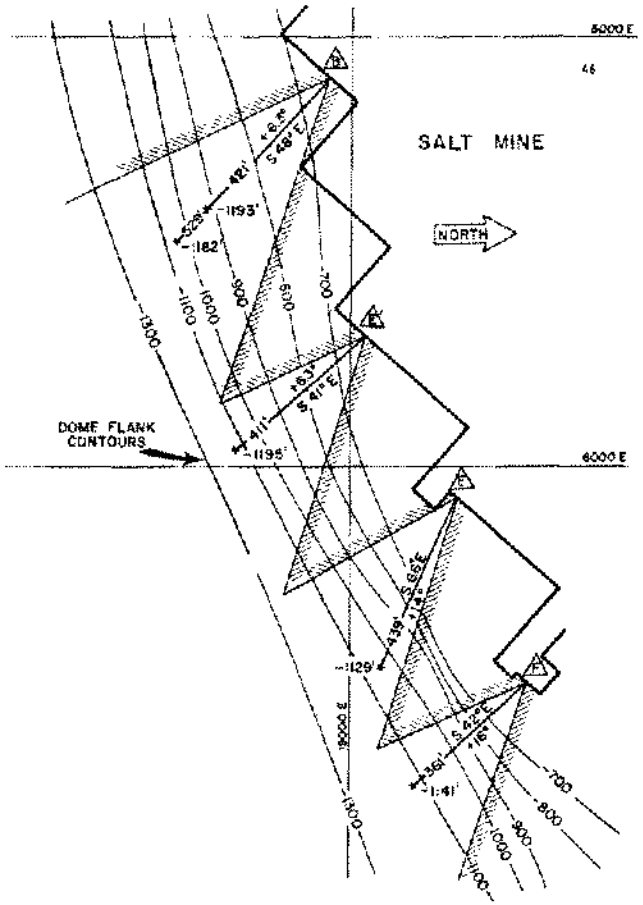

Figure 14. Dome Flank Radar Data.

Figure 13. High Power Radar Antenna Array Probing Upward through Salt at Jefferson Island, La.

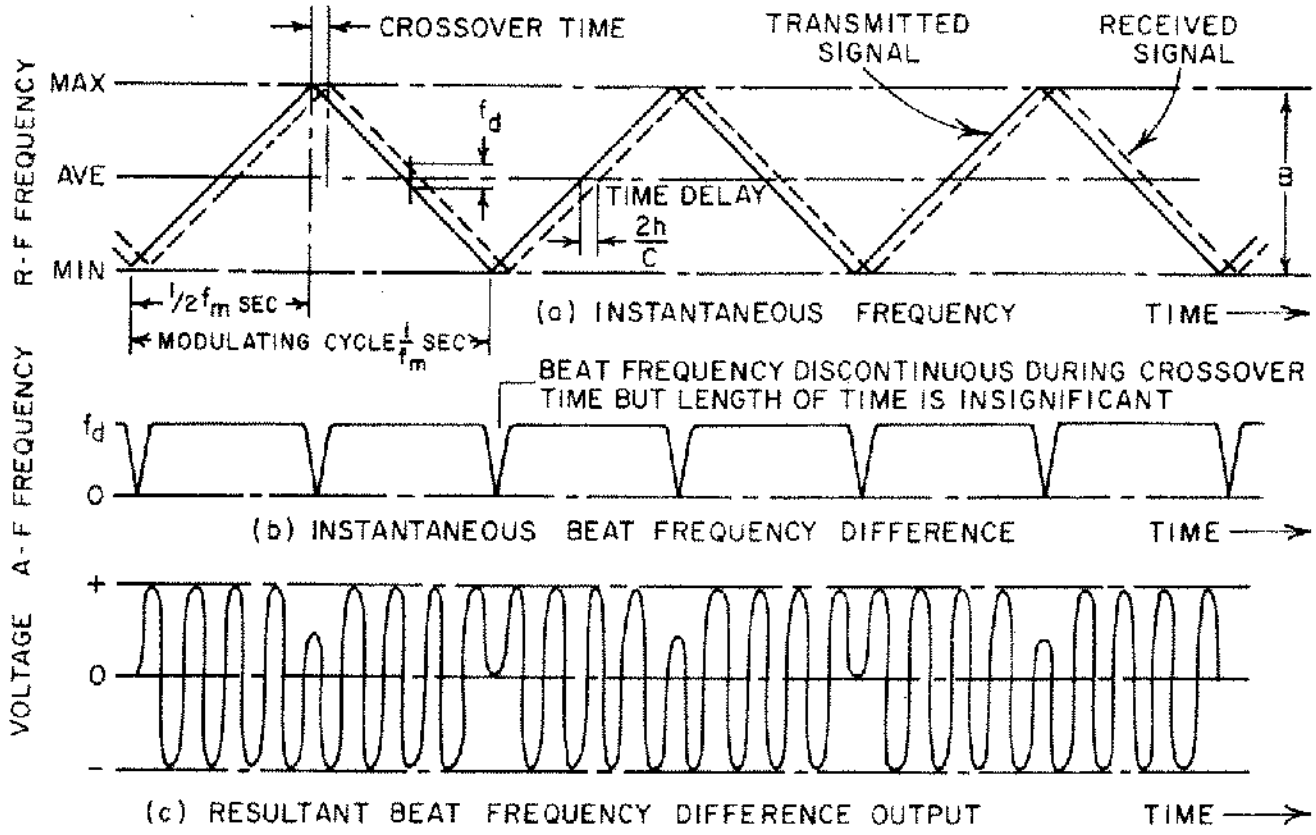

Figure 15. Operation of CW FM Radar.

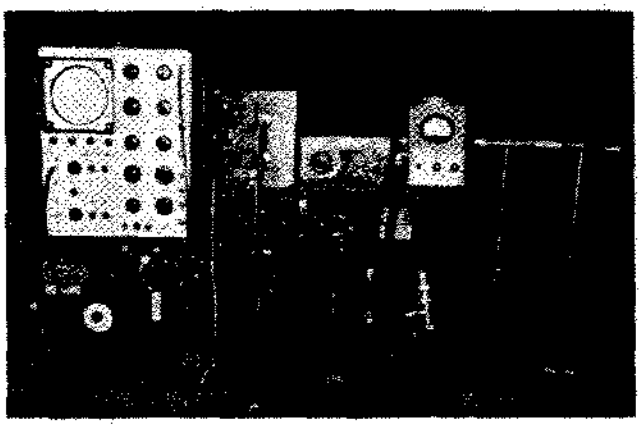

Figure 16. High Power Radar System Less Antennas.

of salt at microwaves is considerably more than at VHF. However, this radar fulfills a distinct need for short range (generally less than 100 feet) high resolution probing into salt.

Examples of this type of radar probing of salt include a probe for the mined out area beneath the floor of salt in the Grand Saline salt mine. Figure 20 shows a plot of the layout of these CW-FM radar probing stations. At each + or x the radar probed into the floor of salt and measured the distance (through salt) to the salt-air interface below. The position known as Station 32 is the location where all these profile lines cross. There is a hole drilled through the floor here so that the thickness of salt here is known to be 13'–8". The East-West profile results were obtained and are shown in Figure 21. The North-South profile results are shown in Figure 22.

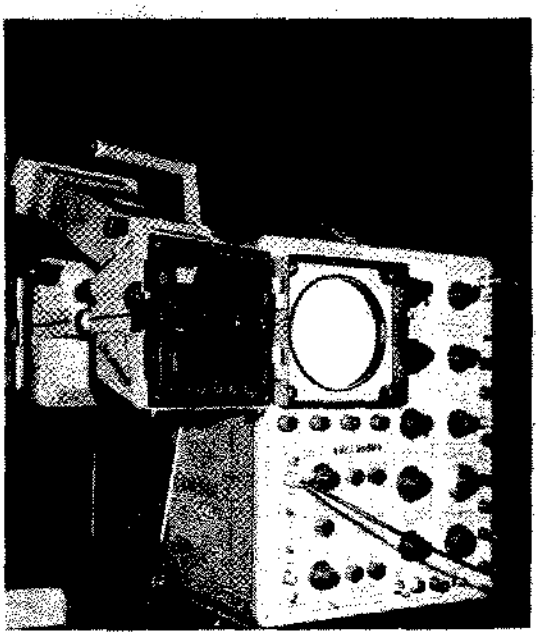

Figure 17. Oscilloscope and Camera for Recording Radar Data.

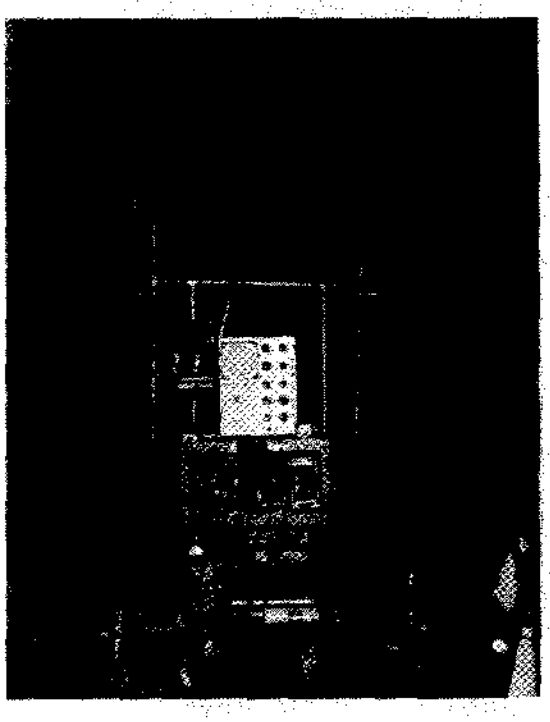

Figure 18. Charlie I Radar System Probing Roof, Jefferson Island Salt Mine.

In another mine in Pugwash, Nova Scotia, a similar profile was carried out but essentially in one direction, namely northeast-southwest. See Figure 23 for the location of the profile substations of radar station 10. Note the two additional substations (small triangles 10 and 11) which form a line essentially at right angles to the long profile. Figure 24 clearly shows the signals received from the air-salt interface on the ceiling of the tunnel beneath the floor. Note in Figure 23 that the tunnel below ends between substations 6 and 7 and that the data of Figure 24 also show the tunnel ending there i.e., no reflections from depths of 30 or more feet at stations 8 and 9.

REFERENCES

Breckenridge, R. G., 1948. Low Frequency Dispersion in Ionic Crystals, *Jour. Chem. Phys.*, 16:959.

Hluckanek, J. A., 1973, M.S. Thesis, Dept. of Geophysics, Texas A & M University, College Station, Texas.

Luck, D. G. C., 1949. *Frequency Modulated Radar.* McGraw-Hill, New York.

Skolnik, M. I., 1962. *Introduction to Radar Systems.* McGraw-Hill, New York.

Unterberger, R. R., 1974. A laser radar for probing salt. *This volume.*

Unterberger, R. R. and J. A. Hluchanek, 1973, Mapping a Salt Dome Top by Electromagnetic Waves from Inside a Salt Dome, paper presented at *Society of Exploration Geophysicists*, Meeting, Mexico City, October.

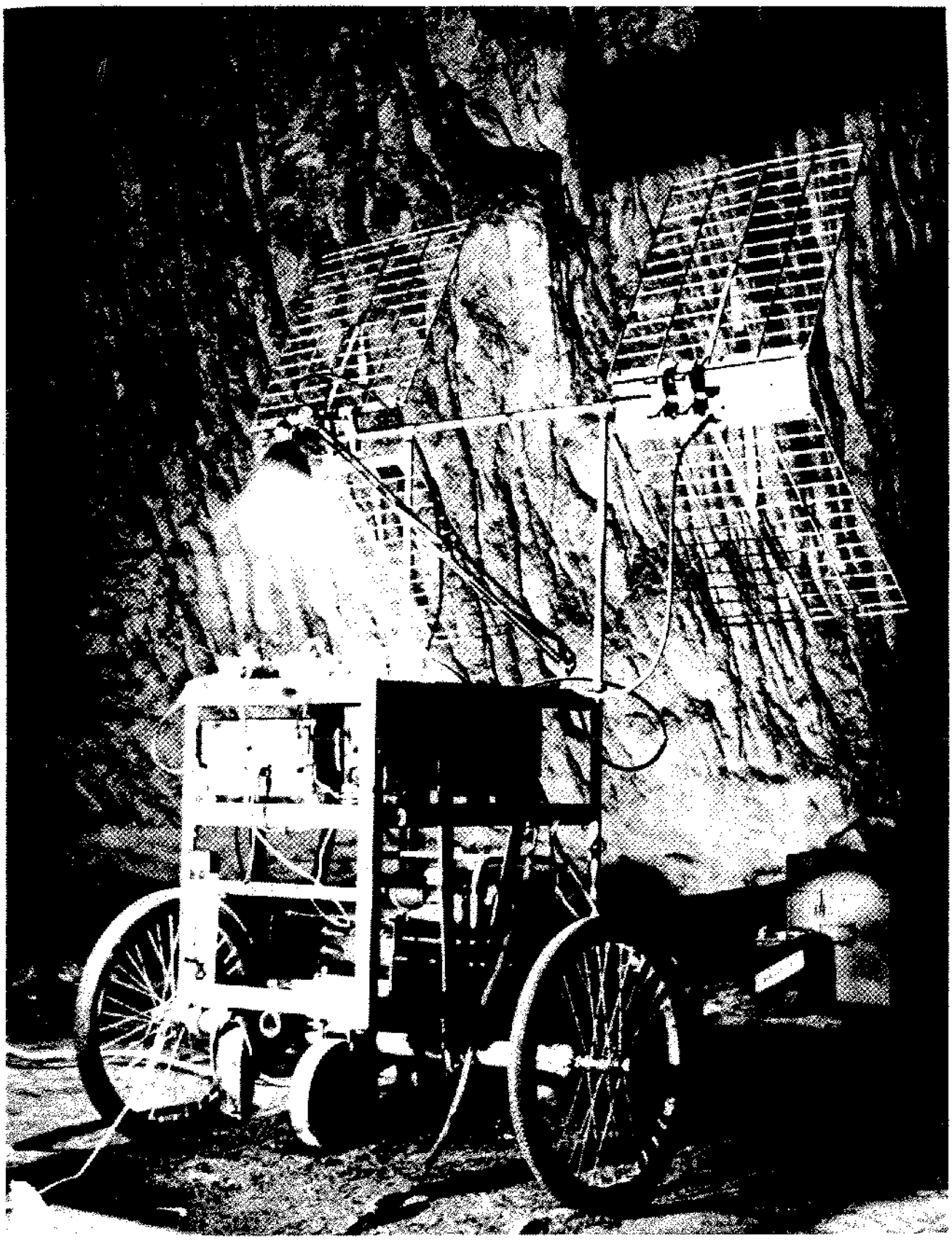

Figure 19. Echo 1 CW-FM Radar System Without Antennas, Goderich Salt Mine.

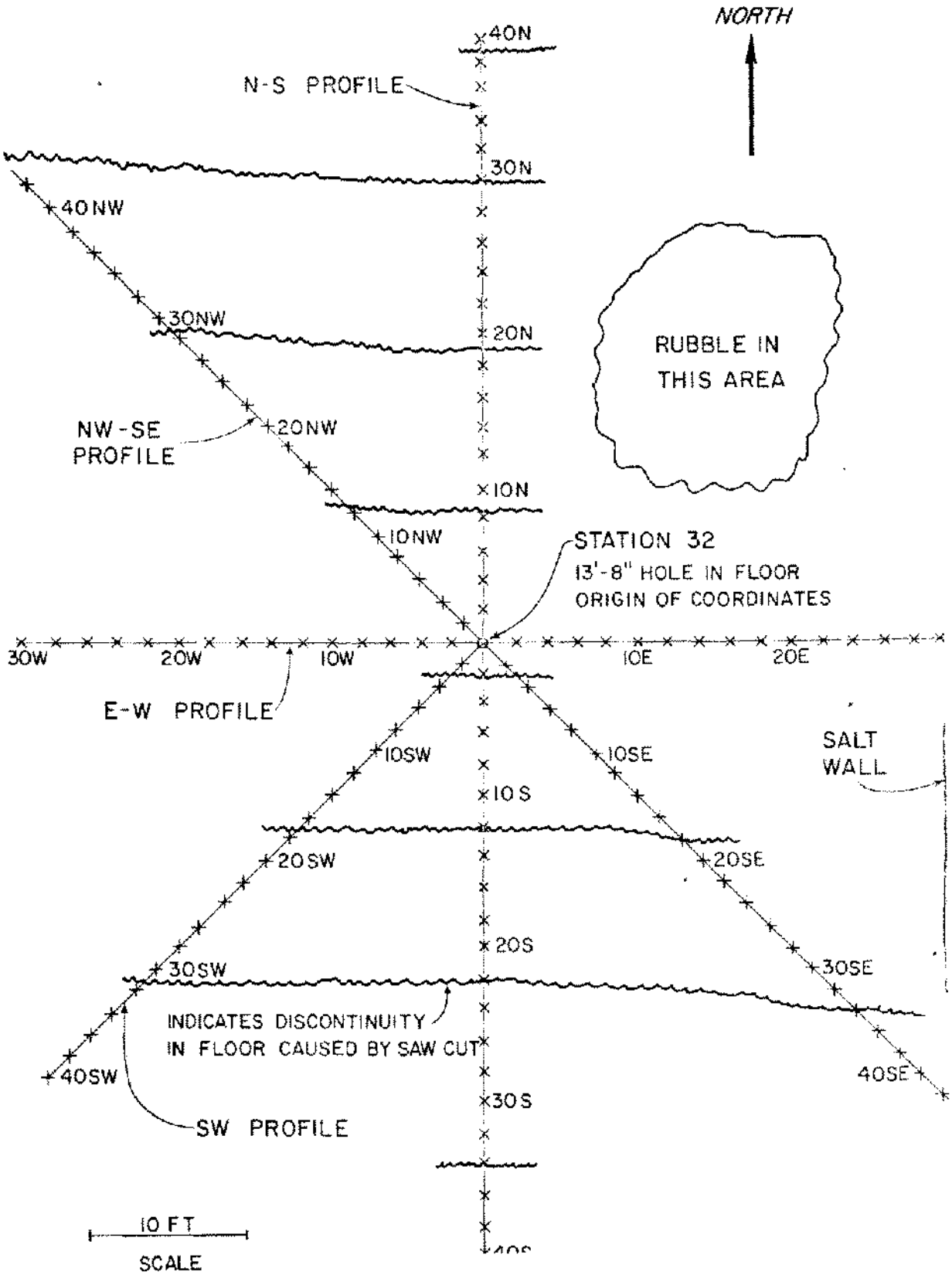

Figure 20. Layout of Station for Detailed Profiling of the Tunnel beneath the salt floor.

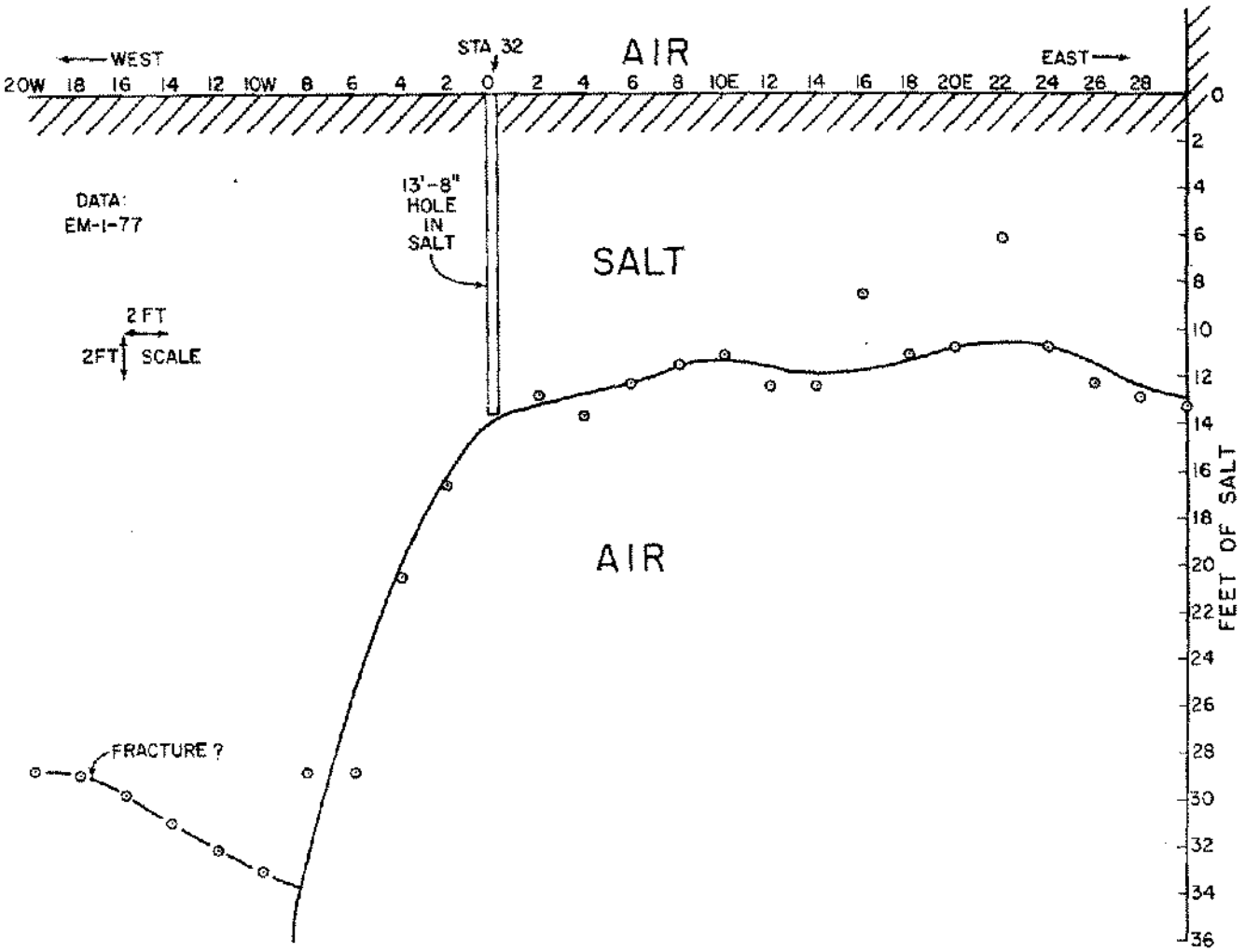

Figure 21. Echo 1 Profile at Station 32: East-West.

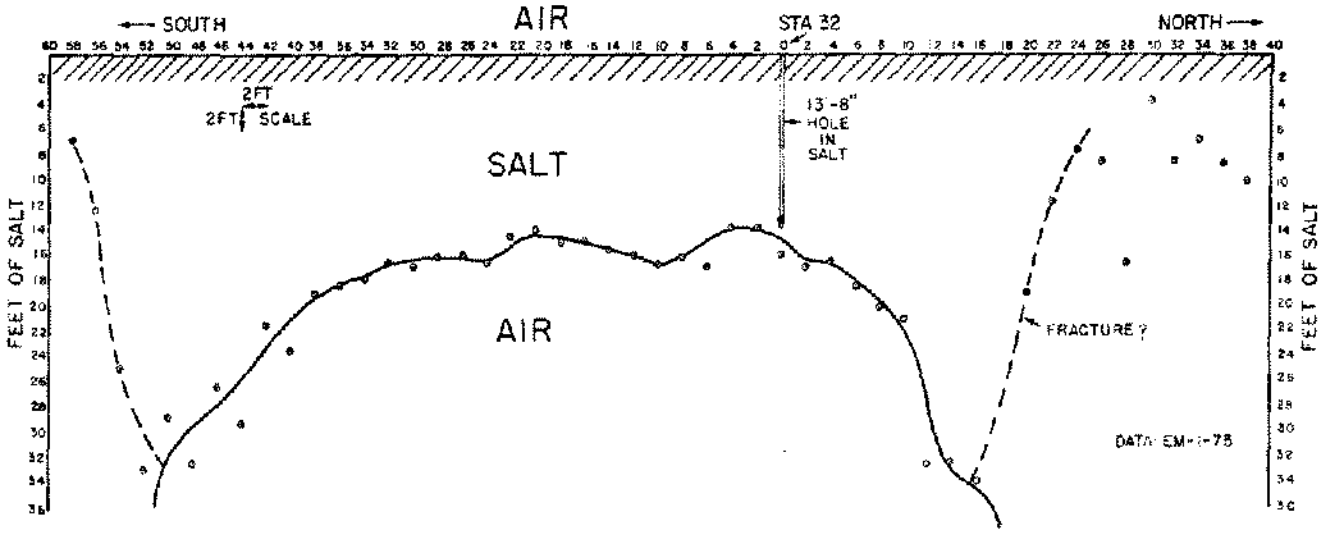

Figure 22. Echo 1 Profile at Station 32: North-South.

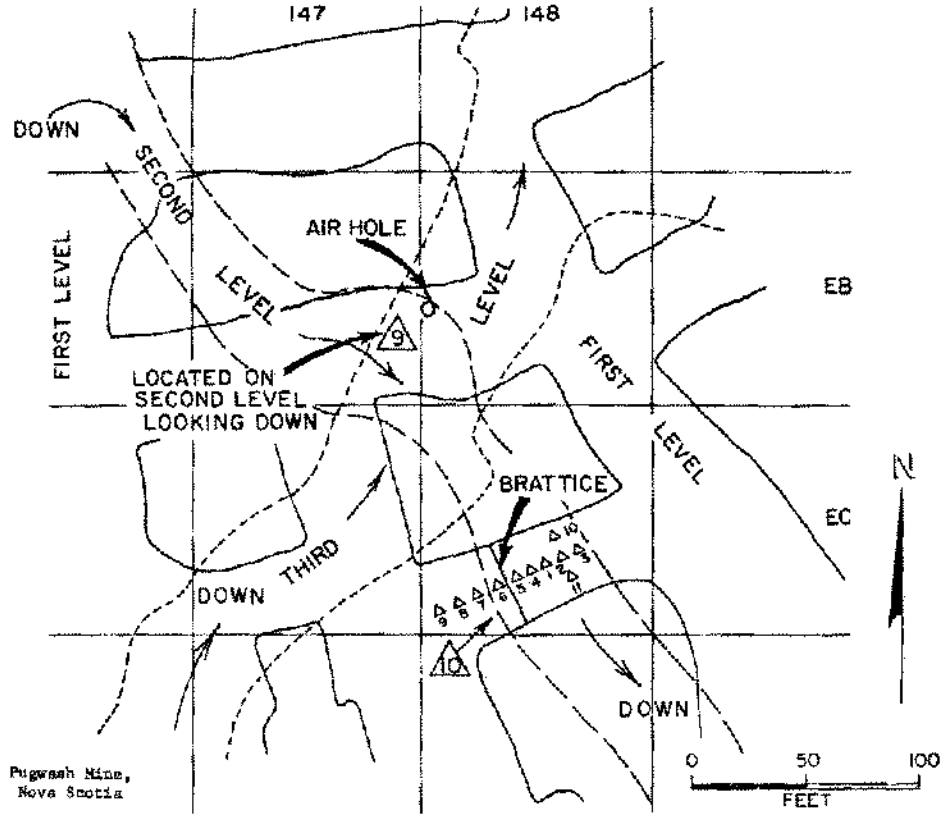

LOCATION OF STATIONS 9 AND 10 WITH SUBSTATIONS

Figure 23. Location of Stations 9 and 10 with Substations.

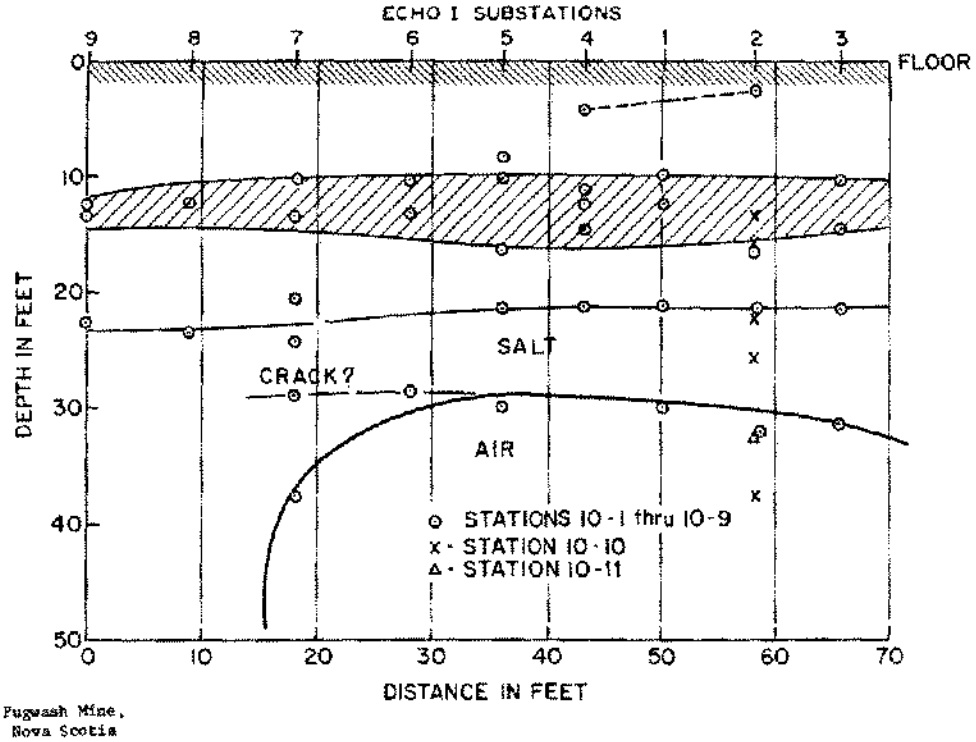

CEILING PROFILE OF LOWER TUNNEL
STATIONS 10-1 THRU 10-11

Figure 24. Ceiling Profile of Lower Tunnel.